1.55 μm room-temperature lasing from subwavelength quantum-dot microdisks directly grown on (001) Si

Bei Shi, Si Zhu, Qiang Li, Chak Wah Tang, Yating Wan, Evelyn L. Hu, and Kei May Lau

Citation: Appl. Phys. Lett. **110**, 121109 (2017); doi: 10.1063/1.4979120
View online: http://dx.doi.org/10.1063/1.4979120
View Table of Contents: http://aip.scitation.org/toc/apl/110/12
Published by the American Institute of Physics

1.55 μm room-temperature lasing from subwavelength quantum-dot microdisks directly grown on (001) Si

Bei Shi,[1,a)] Si Zhu,[1,a)] Qiang Li,[1] Chak Wah Tang,[1] Yating Wan,[1] Evelyn L. Hu,[2] and Kei May Lau[1,b)]
[1]*Department of Electronic and Computer Engineering, Hong Kong University of Science and Technology, Clear Water Bay, Kowloon, Hong Kong*
[2]*School of Engineering and Applied Sciences, Harvard University, Cambridge, Massachusetts 02138, USA*

(Received 26 February 2017; accepted 13 March 2017; published online 22 March 2017)

Miniaturized laser sources can benefit a wide variety of applications ranging from on-chip optical communications and data processing, to biological sensing. There is a tremendous interest in integrating these lasers with rapidly advancing silicon photonics, aiming to provide the combined strength of the optoelectronic integrated circuits and existing large-volume, low-cost silicon-based manufacturing foundries. Using III-V quantum dots as the active medium has been proven to lower power consumption and improve device temperature stability. Here, we demonstrate room-temperature InAs/InAlGaAs quantum-dot subwavelength microdisk lasers epitaxially grown on (001) Si, with a lasing wavelength of 1563 nm, an ultralow-threshold of 2.73 μW, and lasing up to 60 °C under pulsed optical pumping. This result unambiguously offers a promising path towards large-scale integration of cost-effective and energy-efficient silicon-based long-wavelength lasers. *Published by AIP Publishing.* [http://dx.doi.org/10.1063/1.4979120]

Silicon photonics has gone through immense advancements over the past two decades,[1] paving the way towards optoelectronic integrated circuits and inter/intra-chip optical interconnections. Although group-IV-based optical building blocks including silicon modulators,[2] microring resonators,[3] waveguides,[4] and germanium photodetectors[5] have demonstrated their techno-economic viability, an efficient Si-based laser source remains the most challenging component due to the indirect bandgap of Si.[6] Integrating high performance III-V lasers with Si has been considered a promising path to resolve this challenge. Wafer or die bonding has been shown as a successful approach, demonstrating impressive device performances,[7–9] and has gradually been adopted by industry. For large-scale photonic integrations, this method introduces process complexity with some remaining issues.[10] Recently, direct epitaxy of III-V lasers on Si has attracted significant attention with the successful use of self-assembled quantum dots (QDs) as active materials.[11–13] The distinctive zero-dimensional density of states of QDs offers lower threshold current density with improved thermal stability in III-V lasers,[14] and their discrete localization promises greater immunity to defects associated with III-V/Si heteroepitaxy when compared to their conventional quantum-well counterparts.[15] More interestingly, these QDs are capable of bending or pinning the threading dislocations (TDs) because of their large strain field.[16,17]

Recently, high performance electrically pumped continuous-wave InAs/GaAs QD lasers with an emission wavelength as long as 1315 nm have been directly grown on offcut silicon substrates,[11] yielding a low threshold current density of 62.5 A cm^{-2}, and an elevated operation temperature up to 120 °C. These lasers have shown respectable operating lifetimes over 3100 h. To exploit the 1550 nm telecom wavelength where long-distance communication can benefit from the least attenuation, developing InP-based QD lasers on silicon is necessary. In this work, optically pumped subwavelength InAs/In(Al)GaAs quantum dot microdisk lasers (MDLs) epitaxially grown on CMOS-compatible (001) silicon emitting at 1.55 μm are reported. These compact microdisk lasers are advantageous for low power consumption and high quality factor (a few thousands).[6,18] Shrinkage of the disk size opens new venues for future nanophotonic circuits and dense integration. Using QDs as the active medium to effectively counter balance the surface recombination,[19] as well as optimizing the smoothness of the disk sidewall, we are able to overcome the radiative losses and scale the microdisk diameter down to 1.5 μm. With better localized carriers inside the QDs, the internal quantum efficiency of these large surface-to-volume MDLs should be higher than 48%,[20] a theoretical estimate for similar sized MDLs with QWs as gain material. Under pulsed pumping, these subwavelength disks exhibit room-temperature thresholds as low as 2.73 μW and lasing operation up to 60 °C (limited by the measurement setup), with a characteristic temperature as high as 123 K. Statistical analysis based on a variety of disks suggests good device performance when compared with the same microdisk structure on native InP substrates.

All the material growth including the InP-on-Si (IoS) buffer and the microdisk laser structure were completed using an AIX-200/4 metalorganic chemical vapor deposition (MOCVD) system. To fabricate InAs QD MDLs on Si, it is necessary to minimize dislocations that introduce non-radiative recombination and deplete carriers for lasing. Direct epitaxy of InP on Si (~8% lattice mismatch) usually leads to a high density of defects including TDs (10^9–10^{10}/cm^2) and anti-phase-boundaries (APBs).[21] We have employed several

a)B. Shi and S. Zhu contributed equally to this work.
b)Email: eekmlau@ust.hk, Tel.: (852)23587049, Fax: (852) 23581485.

strategies to reduce defect densities, as shown in the cross-sectional transmission electron microscopy (TEM) image (Fig. 1(a)): First, a 1.7-μm-thick GaAs intermediate buffer provides an APB-free III-V surface and accommodates the large mismatch between InP and Si. Inside the GaAs, a ten-stack AlGaAs/GaAs strained-layer superlattice (SLS) was used to reduce dislocation density and to smooth the surface. Secondly, a thin LT-InP nucleation layer (70 nm) was carefully optimized to ensure good island coverage, followed by a 1.4 μm InP single crystal buffer layer deposited at multi-step temperatures. A 60 nm $In_{0.6}Ga_{0.4}As$ strained interlayer was inserted to filter the dislocations generated at the interface of InP/GaAs.[22] A typical $5 \times 5\ \mu m^2$ atomic force microscopy (AFM) image of the as-grown InP buffer surface (Fig. 1(e)) shows a smooth morphology with root-mean square roughness of 1.6 nm. MDL consisting of a seven-period InAs/InGaAs/InAlGaAs dot-in-well (DWELL) structure sandwiched by InAlAs claddings (Fig. 1(b)) was grown on the APB-free IoS templates.[23] Figure 1(c) presents a close-up TEM image of the MDL epi-structure on silicon. The InAs QDs with a typical diameter of ~45 nm (Fig. 1(d)) were grown on top of a strained InGaAs wetting layer and immediately capped by a thin LT-InAlGaAs (1.5 nm) to avoid desorption. Then, a thick high-temperature (HT) InAlGaAs spacer (52 nm) was deposited to anneal these truncated QDs, preventing dot height dispersion and tuning the emission wavelength. A representative AFM image of the uncapped InAs QDs on the IoS substrate is illustrated in Fig. 1(d), with a density of $\sim 4 \times 10^{10}\,cm^{-2}$. A few large clusters resulting from the bumpy InP underneath were identified. For benchmarking, the same MDL structure was also grown on an InP (001) native substrate in the same growth run. Normalized room-temperature photoluminescence (RT-PL) of both samples centered at ~1500 nm is shown in Fig. 1(f). The peak intensity for the MDL on IoS was 3.5 times lower than the one grown on InP, with a shoulder apparent in the higher energy side, which can be attributed to the dot size fluctuation.[24] The broad spectra however favor the interaction between resonant modes in small cavities and the material gain.

Ultra-small MDLs (1.5 μm in diameter) were fabricated using the colloidal lithography method.[25] Dry-etch was performed to define the disk region and was terminated at the InP buffer layer, followed by a selective wet-etch to form the InP pillar. A typical 70° tilted scanning electron microscope (SEM) image in the inset of Fig. 3(c) clearly reveals a smooth and steep sidewall, as well as a cylindrical geometry. The well-developed fabrication process greatly benefits the whispering-gallery mode (WGM) oscillation around the disk periphery, enabling these devices to operate above room temperature.

Figure 2(a) shows the room temperature emission spectra of an as-fabricated MDL. The micro-PL measurements were performed using a 532 nm Q-switched Nd:YAG pulsed laser source (20 ns pulse width, 3000 Hz repetition rate). The average input power reaching the top surface of MDLs was calibrated by a power-meter. At a low excitation power of 2.1 μW, a weak cavity mode started to emerge. Meanwhile, linewidth narrowing phenomenon was observed as the pump power increased below the lasing threshold (Fig. 2(b)). Further increase of the injection power led to stimulated emission at ~1563 nm with a high background suppression ratio of 21.7 dB, as shown in the inset of Fig. 2(a). In addition, the linewidth of the lasing peak enlarged as the pump power was raised above the threshold due to wavelength chirping, which was associated with changes in refractive index induced by transient changes of carrier density in the QDs.[26] The cold cavity quality factor is calculated by $Q = \lambda/\triangle\lambda \sim 1563$. In the inset of Fig. 2(a), no peak wavelength shift can be observed with progressively increased pumping power, suggesting negligible thermal generation inside the disk region and good dissipation through the InP pillar and the IoS substrate. Figure 2(b) demonstrates the integrated output intensity as a function of injection power (L-L curve), with a clear "kink" appearing at the lasing threshold (P_{th}) of $2.73 \pm 0.23\ \mu W$. Note that this value of threshold represents the upper bound, without accounting for multiple reflection/absorptions inside the disk and coupling efficiency of the pump beam. This ultralow threshold promises minimal

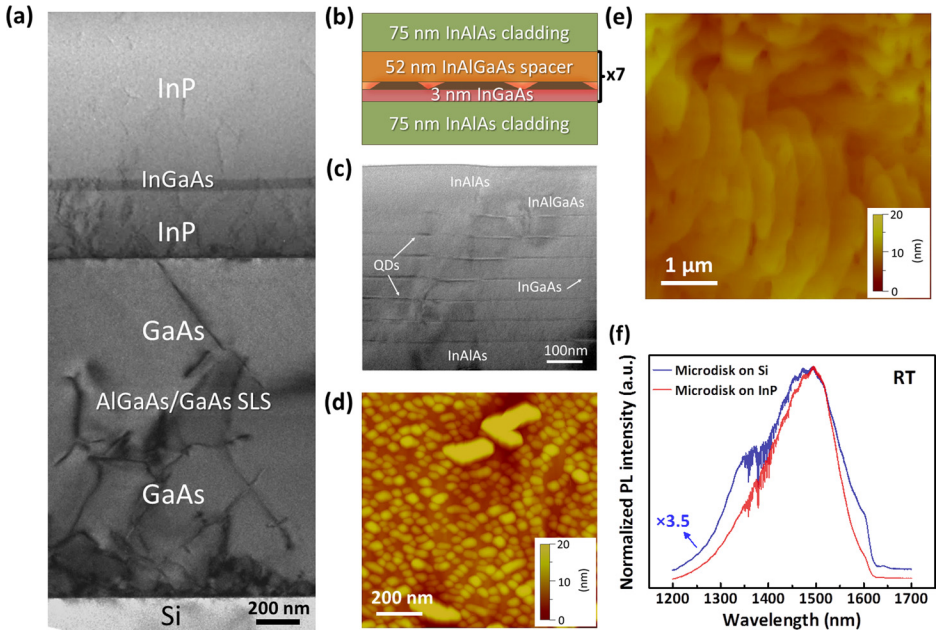

FIG. 1. (a) Cross-sectional TEM image of the InP-on-Si template; (b) Schematic diagram of the microdisk laser structure; (c) Zoomed-in TEM of the microdisk laser on Si, highlighting the InAs/InGaAs/InAlGaAs DWELLs; (d) Representative surface morphology of uncapped InAs QDs on top of the InP-on-Si substrate, with a few large clusters observed; (e) Typical $5 \times 5\ \mu m^2$ AFM image of the surface of InP thin film grown on Si, showing a step-flow morphology with a low root-mean square roughness of 1.6 nm; (f) Room-temperature photoluminescence of the as-grown microdisk laser samples on Si and InP substrates, respectively.

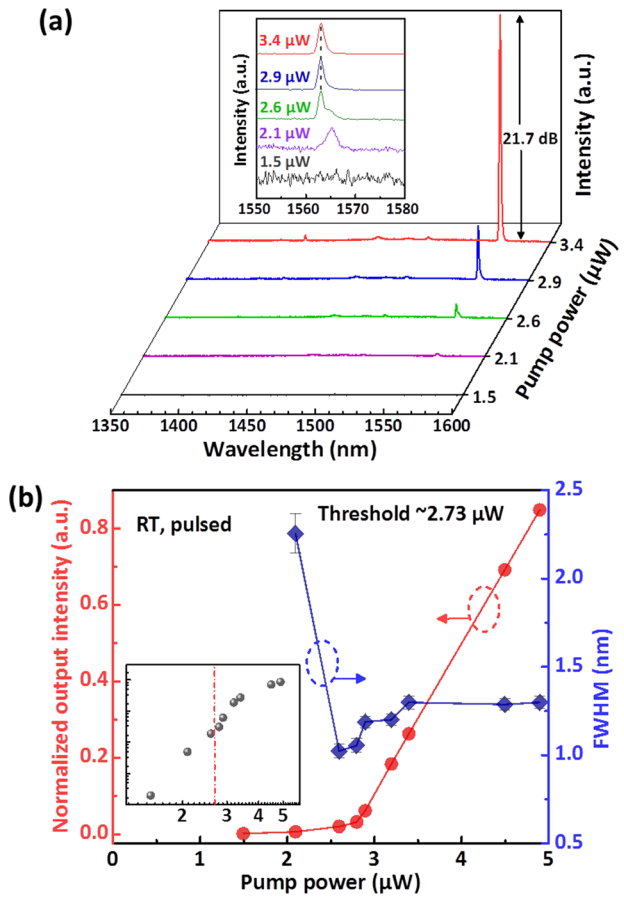

FIG. 2. (a) Emission spectra as pulse pumping progressively increases to demonstrate single-mode lasing at 1563 nm. Inset: Zoomed-in spectra at various injection powers to reveal no peak wavelength shift with enlarging pump power; (b) Linewidth evolution and normalized output intensity as a function of pumping power (L-L curve). Inset: Double-logarithmic plot of the L-L curve, with red dashed line distinguishing spontaneous and stimulated emission.

power consumption for subwavelength lasers. A logarithmic plot of the L-L curve in the inset image exhibits the "S-shaped" nonlinear transition from spontaneous emission to lasing.[26]

Statistical analysis based on a random sampling (ten lasers for each sample) of MDLs on the IoS template and InP substrate was conducted for a fair comparison of the lasing thresholds, considering the variations in the microdisk fabrication processes. 4-μm-diameter disks were fabricated simultaneously as references to investigate the dependence of device performance when the disk size shrinks to subwavelength dimensions. The statistical lasing thresholds as a function of wavelength for the 1.5-μm and 4-μm disks are shown in Figs. 3(a) and 3(b), respectively. In both cases, the average thresholds for the MDLs on silicon are about twice the average values of those on InP substrates. The larger thresholds on silicon are mainly associated with three factors. First, the material gain in the QD active region on silicon is somewhat lower due to non-radiative recombination processes introduced by crystalline defects. Second, the injection efficiency is reduced because the pump laser generated carriers can be partially trapped by the deep energy level traps related with dislocations in the disk region.[13] Moreover, the broader PL emission spectrum of the MDL on silicon is more favorable for multi-mode lasers (Fig. 1(f)). It is noted in Fig. 3(a) that single-mode lasers (solid circles) among the measured devices on silicon generally exhibit lower thresholds than their multi-mode counterparts (open circles) due to mode competition. Figure 3(b) clearly shows that as the disk diameter increases, the thresholds become larger for MDLs on both substrates. Understandably, smaller active volume in a subwavelength MDL requires less pump power for lasing, leading to a lower threshold. Conversely, the free spectral range (FSR) increases as the disk size diminishes ($\mathrm{FSR} = \lambda^2/2\pi r n_{eff} \approx 142$ nm for d = 1.5 μm, and $\sim$53 nm for d = 4 μm). Smaller mode separation for larger disks is more inclined to show multi-mode lasing (open symbols in Fig. 3(b)). Here, only the lowest radial order modes with different azimuthal mode numbers ($\mathrm{TE}_{1,6}$ and $\mathrm{TE}_{1,7}$ modes in Fig. 3(c) denote radial mode number $l = 1$, and azimuthal mode number $m = 6$ or 7) appear in the 1.5 μm MDLs because higher radial order modes may easily be coupled into the supporting post (undercut $\sim$270 nm). This is further verified by numerical simulation of the exact device topology using finite-difference time-domain (FDTD) method. The inset of Fig. 3(c) demonstrates a three-dimensional view of the electric field distribution of the $\mathrm{TE}_{1,6}$ WGM, illustrating most of the electric field confined around the periphery of the disk and the evanescent field that introduces radiative losses. Figure 3(c) overlays one of the typical multi-mode lasing spectra with their threshold powers of four MDLs. Matching the

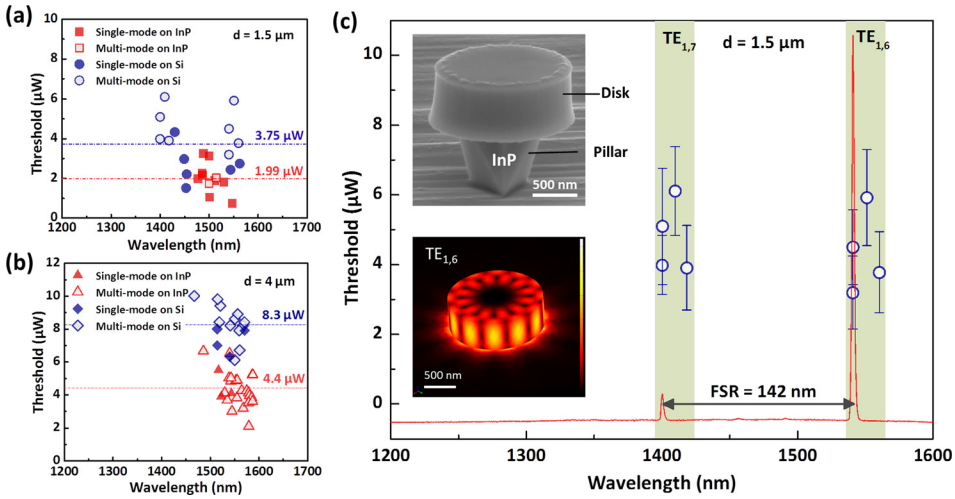

FIG. 3. Single-mode (solid symbols) and multi-mode (open symbols) lasing thresholds dispersion of (a) 1.5-μm and (b) 4-μm microdisks on InP and Si as a function of wavelength; (c) An overlay of threshold powers in multi-mode 1.5-μm disks (error bars introduced) with a representative lasing spectrum, illustrating the two adjacent modes in the lowest radial order. The top inset SEM image clearly shows the good device topology of the fabricated subwavelength MDL, while the bottom inset is a three-dimensional electric field distribution of the simulated $\mathrm{TE}_{1,6}$ mode.

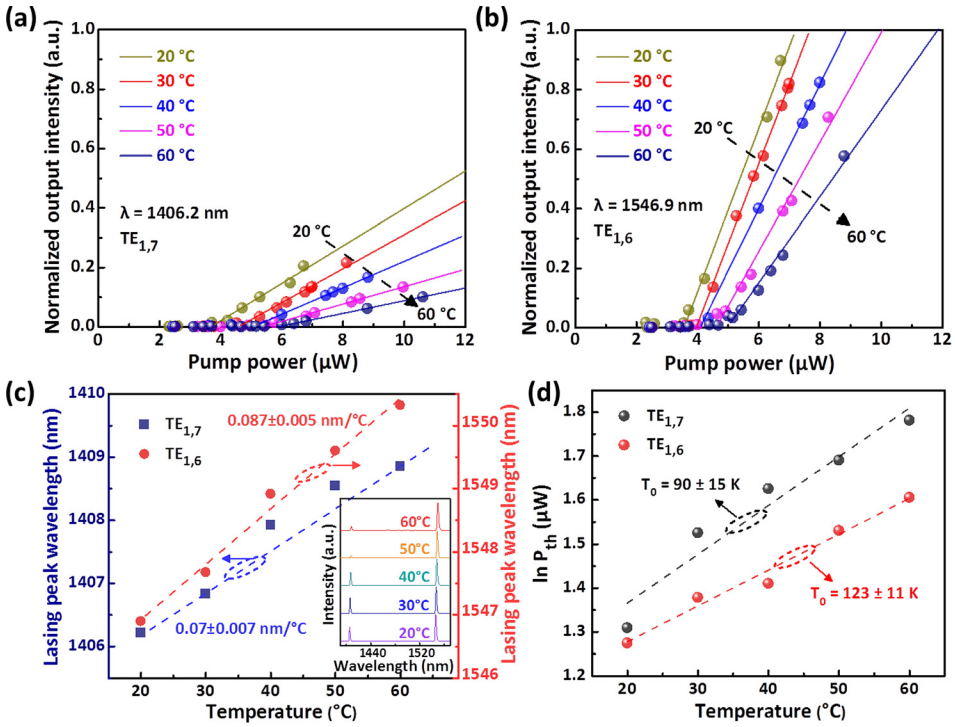

FIG. 4. Normalized output intensity versus input power for (a) $TE_{1,7}$ and (b) $TE_{1,6}$ modes with substrate temperature ranging from 20–60 °C; (c) peak wavelength redshifts as the temperature increases for both modes (the inset presenting emission spectra when pump power doubles the thresholds); (d) linear fit to the thresholds as a function of temperature to extract the characteristic temperatures T_0.

peak wavelengths with the simulation results clearly reveals that the two lasing modes are in the first radial order with adjacent azimuthal mode numbers, and the separation is equal to a FSR. Dispersion in the peak wavelength is a result of disk diameter fluctuation in fabrication.

In addition to the extremely low thresholds (P_{th}), it is of great importance for lasers to operate at chip temperatures. Figures 4(a) and 4(b) display a set of L-L curves at various substrate temperatures ranging from 20 °C to 60 °C, for the $TE_{1,7}$ and $TE_{1,6}$ modes respectively. No heat sinks or heat dissipations were applied to the lasers. It should be pointed out that the lasers remain lasing at an elevated chip temperature above 60 °C, limited by the measurement setup. Compared with the $TE_{1,7}$ mode on the higher energy side (1406.2 nm), the slope efficiency of the $TE_{1,6}$ mode (1546.9 nm) is larger with a higher output intensity under the same pumping condition, suggesting (1) higher capture efficiency in larger QDs,[27] and (2) reabsorption of higher energy photons before coupling to cavity modes.[28] Figures 4(c) and 4(d) highlight the lasing peak wavelengths and thresholds of these two modes as a function of substrate temperature, respectively. First, the lasing wavelengths redshift by 0.07–0.09 nm/°C in the temperature range of 20–60 °C for both modes, resulting from the InAs bandgap shrinkage and temperature-induced cavity effective refractive index change.[27] The different wavelength variations with temperature for the two modes can be explained by different effective refractive index change coefficients ($\triangle n_c$) as a function of temperature.[29] Inset of Fig. 4(c) presents the zoomed-in emission spectra as the substrate temperature was ramped up with the pump power doubling the lasing thresholds, offset vertically for clarity. The intensity ratio of $TE_{1,6}$ to $TE_{1,7}$ becomes larger at a higher temperature ($P_{pump} = 2 \times P_{th}$), because of the temperature redshift in the material gain. A high characteristic temperature, $T_0 \approx 123$ K in the range of 20–60 °C was extracted for the $TE_{1,6}$ mode in Fig. 4(d), which is among the best reported T_0 for QD MDLs on III-V substrates.[19,25,27] The temperature-insensitive characteristics demonstrated here can potentially promote their applications in silicon photonics. Here, the larger T_0 of the $TE_{1,6}$ mode can be attributed to a better overlap with the gain spectrum at higher temperatures and a superior carrier capture efficiency in larger QDs,[27] which prevent carrier evaporation into barriers.

In summary, we have demonstrated 1550 nm subwavelength quantum dot microdisk lasers monolithically grown on (001)-Si substrates. Room-temperature pulsed lasing has been achieved with an extremely low threshold of 2.73 μW by combining the small microdisk cavity and quantum dots. These ultra-small lasers can operate at an elevated temperature beyond 60 °C, with a large characteristic temperature of 123 K. This approach therefore indicates the feasibility of directly grown on-chip light sources for Si photonics and holds promise for low-cost, large-scale, and high-density photonic integrated circuits. Continuous effort is being made on further improved InP/Si buffer and more uniform QDs with a higher dot density, which will produce high-efficiency electrically injected p-doped QD lasers.

This work was supported in part by Grants (Nos. 614813 and 16212115) from the Research Grants Council of Hong Kong. The authors would like to thank Professor J. Xia and his team in Wuhan National Laboratory for Optoelectronics (WNLO) for providing facilities to perform laser measurements, Professor D. Bimberg, J.-H. Schulze and D. Quandt for growth guidance, Professor J. E. Bowers and B. Lai for fruitful discussions, and the NFF, MCPF of HKUST for technical support.

[1]D. Liang and J. E. Bowers, Nat. Photonics **4**, 511–517 (2010).
[2]Y. Jiang, W. Jiang, L. Gu, X. Chen, and R. T. Chen, Appl. Phys. Lett. **87**, 221105 (2005).
[3]K. Preston, P. Dong, B. Schmidt, and M. Lipson, Appl. Phys. Lett. **92**, 151104 (2008).

[4]G. Roelkens, D. Vermeulen, D. Van Thourhout, R. Baets, S. Brision, P. Lyan, P. Gautier, and J. M. Fedeli, Appl. Phys. Lett. **92**, 131101 (2008).
[5]D. Feng, S. Liao, P. Dong, N. N. Feng, H. Liang, D. Zheng, C. C. Kung, J. Fong, R. Shafiiha, J. Cunningham, and A. V. Krishnamoorthy, Appl. Phys. Lett. **95**, 261105 (2009).
[6]D. Liang, X. Huang, G. Kurczveil, M. Fiorentino, and R. G. Beausoleil, Nat. Photonics **10**, 719–722 (2016).
[7]C. Seassal, P. Rojo-Romeo, X. Letartre, P. Viktorovitch, G. Hollinger, E. Jalaguier, S. Pocas, and B. Aspar, Electron. Lett. **37**, 222–223 (2001).
[8]J. Van Campenhout, P. Rojo-Romeo, P. Regreny, C. Seassal, D. Van Thourhout, S. Verstuyft, L. Di Cioccio, J. M. Fedeli, C. Lagahe, and R. Baets, Opt. Express **15**, 6744–6749 (2007).
[9]K. Tanabe, K. Watanabe, and Y. Arakawa, Sci. Rep. **2**, 349 (2012).
[10]J. P. Reithmaier and M. Benyoucef, ECS Trans. **72**, 171–179 (2016).
[11]S. Chen, W. Li, J. Wu, Q. Jiang, M. Tang, S. Shutts, S. N. Elliott, A. Sobiesierski, A. J. Seeds, I. Ross, P. M. Smowton, and H. Liu, Nat. Photonics **10**, 307–311 (2016).
[12]A. Y. Liu, C. Zhang, J. Norman, A. Snyder, D. Lubyshev, J. M. Fastenau, A. W. Liu, A. C. Gossard, and J. E. Bowers, Appl. Phys. Lett. **104**, 041104 (2014).
[13]Y. Wan, Q. Li, A. Y. Liu, W. W. Chow, A. C. Gossard, J. E. Bowers, E. L. Hu, and K. M. Lau, Appl. Phys. Lett. **108**, 221101 (2016).
[14]M. Sugawara and M. Usami, Nat. Photonics **3**, 30–31 (2009).
[15]A. Y. Liu, S. Srinivasan, J. Norman, A. C. Gossard, and J. E. Bowers, Photonics Res. **3**, B1–B9 (2015).
[16]J. Yang, P. Bhattacharya, and Z. Mi, IEEE Trans. Electron Devices **54**, 2849–2855 (2007).
[17]H. Liu, T. Wang, Q. Jiang, R. Hogg, F. Tutu, F. Pozzi, and A. Seeds, Nat. Photonics **5**, 416–419 (2011).
[18]M. T. Hill and M. C. Gather, Nat. Photonics **8**, 908–918 (2014).
[19]T. Ide, T. Baba, J. Tatebayashi, S. Iwamoto, T. Nakaoka, and Y. Arakawa, Opt. Express **13**, 1615–1620 (2005).
[20]K. Nozaki and T. Baba, IEEE J. Sel. Areas Commun. **23**, 1411–1417 (2005).
[21]B. Shi, Q. Li, and K. M. Lau, J. Cryst. Growth **464**, 28–32 (2017).
[22]M. Li, H. Li, C. W. Tang, and K. M. Lau, IEEE Electron Device Lett. **33**, 498–500 (2012).
[23]B. Shi, S. Zhu, Q. Li, Y. Wan, E. L. Hu, and K. M. Lau, ACS Photonics **4**, 204–210 (2017).
[24]A. Tackeuchi, Y. Nakata, S. Muto, Y. Sugiyama, T. Inata, and N. Yokoyama, Jpn. J. Appl. Phys., Part 2 **34**, L405 (1995).
[25]S. Zhu, B. Shi, Y. Wan, E. L. Hu, and K. M. Lau, Opt. Lett. **42**, 679–682 (2017).
[26]J. Tatebayashi, S. Kako, J. Ho, Y. Ota, S. Iwamoto, and Y. Arakawa, Nat. Photonics **9**, 501–505 (2015).
[27]Y. Wan, Q. Li, A. Y. Liu, A. C. Gossard, J. E. Bowers, E. L. Hu, and K. M. Lau, Appl. Phys. Lett. **109**, 011104 (2016).
[28]A. C. Tamboli, E. D. Haberer, R. Sharma, K. H. Lee, S. Nakamura, and E. L. Hu, Nat. Photonics **1**, 61–64 (2007).
[29]T. Ma, J. Yuan, L. Sun, Z. Kang, B. Yan, X. Sang, K. Wang, Q. Wu, H. Liu, J. Gao, and C. Yu, IEEE Photonics J. **9**, 1–13 (2017).